preprint to be published in the proceedings of the
26th European Photovoltaic Solar Energy Conference, 5–9 September 2011, Hamburg, Germany

MODELLING VOLUME RATIO, GRADIENT AND LIGAND LAYER THICKNESS OF QUANTUM DOT – POLYMER SOLAR CELLS

M. Schädel[a,b], K. J. Jeltsch[a], A. Kiesow[c], Y. Zhou[d], M. Krüger[d], K. Meerholz[a]
a) Universität zu Köln, Department für Chemie, Luxemburgerstr. 116, D-50939 Köln
b) Q-Cells SE, OT Thalheim, Sonnenalle 17-21, D-06766 Bitterfeld-Wolfen
tel: +49(0)34946699-51139, fax: +49(0)34946699-51100, m.schaedel@q-cells.com
c) Fraunhofer Institute for Mechanics of Materials, Walter-Hülse-Str. 1, D-06120 Halle
d) Laboratory for Nanosciences, Freiburg Materials Research Center (FMF),
Universität Freiburg, Stefan Meier Straße 21, D-79104 Freiburg

ABSTRACT: The optical constants of different conjugated polymers and CdSe nanoparticles (NP) are analysed using spectroscopic ellipsometry. These results are used to model their blends by effective medium approximation (EMA) with a strongly reduced number of parameters. As a result of these models, the volume ratio of the blended components and gradients of the composition along the film thickness are found. The gradients are confirmed by high-resolution transmission electron microscopy. In combination with the mass ratio of the blend the determined volume ratio leads to the mass density of the NP species. This allows for the analysis of the capping ligand on the NP surface in the sub-nanometer range.
Keywords: Modelling, Organic Solar Cell, Quantum Dots, Nanoparticles, Heterojunction

1 INTRODUCTION

The progress in organic photovoltaics led to power conversion efficiencies (PCE) above 8% so far [1]. The photoactive components of such cells consist of blended or stacked heterojunctions of conjugated polymers and fullerenes. Fullerenes and their derivates comprise many advantages like high electron mobility and the self-organised formation of domains and pathways for the electrons to reach the contacts [2]. However, the light absorption of the fullerenes is rather poor with respect to solar radiation. Thus, in such devices light harvesting is limited by the polymer absorption spectra.

In order to further increase the solar cell performance many efforts have been made to replace the fullerene. Promising candidates are inorganic nanoparticles (NP) based on compound semiconductors [3]. The optical and electrical properties in such particles are tuneable by variations in size, shape and surface treatment [4]. A widespread species is CdSe, leading to PCE of 2.7% for spherical quantum dot (QD) [5], 3.2% for tetrapods [6] and 3.5% for combined QD and nanorods (NR) [7]. During the synthesis of the NP an organic ligand is capping the surface. This ligand layer is required for solubility in common solvents as well as for passivation of the disordered semiconductor surface [4]. The ligand also affects the film morphology and the inter- and intra-species electronic transport [4].

This paper presents characterisation methods for the morphology of different polymer/QD blend films. The analysis is based on modelling spectroscopic ellipsometry data with an effective medium approximation (EMA). This allows for the evaluation of volume ratios and gradients of the composition along the blend film thickness. The volume and mass ratio comprise information on the mass density of the ligand species. Using a geometrical model this allows for the evaluation of the ligand layer thickness.

2 EXPERIMENTAL

2.1 Synthesis and sample preparation

We tested several types of QD and NR prepared in different labs and by different routines. For QD with pyridine ligand we used a flow-through microreactor system comparable to a reported one [8] and a mixture of trioctylphosphine (TOP) and oleic acid (OA) as synthesis ligand. The NR were synthesised according to the published procedure [9]. For ligand exchange the particles were treated by methanol and stirred in n-hexane for at least 12 hours and again washed by methanol twice. The washed nanoparticles were refluxed in pyridine at 108 °C for 8 hours [10].

For QD with hexanoic acid (HA) treated hexadecylamine (HDA) 0.4 mmol Cd-stearat, 12 mmol HDA and 8 mmol TOP-OA were loaded in a reaction flask. After heating to 330 °C, 0.4 ml of a 1 M solution of Se in TOP was rapidly injected. The solution was then maintained at 330 °C for 30 minutes to allow the growth of CdSe QD with HDA synthesis ligand. 1 ml of this product were mixed with 6 ml HA and 12 ml methanol at 105 °C. The precipitate QD were recovered by centrifugation. 1 ml chloroform and 3 ml methanol were added at 85 °C. Again the precipitate QD were recovered by centrifugation, and then dispersed into anhydrous chlorobenzene (CB). This procedure is also reported in [5] and [11].

We used the polymers poly(3-hexylthiophene) (P3HT) (M_n = 13 kg mol^{-1}, Merck EF-430302), poly[2,6-(4,4-*bis*(2-ethylhexyl)-*4H*-cyclopenta [2,1-*b*;3,4-*b'*]dithiophene-*alt*-2,6-(4,8-dioctyloxybenzo [1,2-*b*;4,5-*b'*]dithiophene] (PCPDTBDT) and the low band gap polymer poly[2,6-(4,4-bis-(2-ethylhexyl)-*4H*-cyclopenta[2,1-*b*;3,4-*b'*]dithiophene)-*alt*-4,7-(2,1,3-benzothiadiazole)] (PCPDTBT). PCPDTBT and PCPDTBDT were synthesized in Stille-type cross coupling polycondensations according to published procedures [12] with mean average molecular weights M_n of 15 kg mol^{-1} (PCPDTBT) and 38 kg mol^{-1} (PCPDTBDT).

All devices were fabricated on commercial indium-tin oxide (ITO) coated glasses. The ITO was masked and etched with ferric chloride / hydrochloric acid and subsequently cleaned using chloroform, acetone, Mucasol detergent, and deionized water in an ultrasonic bath. Next, the ITO substrates were exposed to ozone for 15 min and immediately coated with poly(3,4-

ethylenedioxythiophene) poly(styrenesulfonate) (PEDOT:PSS, CLEVIOS HIL 1.3). Afterwards the samples were heat treated for 2 min at 110 °C to remove residual water. The blend films were spin-coated from chlorobenzene in an N_2-filled glove box. P3HT, PCPDTBT and PCPDTBDT were dissolved in CB with a concentration of 15-20 mg mL^{-1}.

2.2 Spectroscopic Ellipsometry

The optical measurements were performed with a J. A. Woollam M2000 rotating compensator ellipsometer with wavelength range from 240 nm to 1700 nm, and angles of incidence between 55° and 85°. In addition, the transmitted light intensity was measured under different polarisation and perpendicular angle of incidence. After the optical measurements step height profiles (DEKTAK) were taken along a scratch on the investigated areas. The determined layer thickness was used as start value and reference for the optical models.

Due to masked etching of the ITO two different optical settings were obtained: Glas (1 mm) / ITO (150 nm) / PEDOT:PSS (30 nm) / layer of interest and Glas (1 mm) / PEDOT:PSS (30 nm) / layer of interest. Due to the absence of ITO in the second case a second independent set of information is obtained. The surface for the layer of interest is in both cases PEDOT:PSS. Thus, surface energy or morphology-dependent changes in optical constants as reported in other studies [13] can be excluded. The substrate systems were previously carefully analysed and kept constant during the modelling of the layer of interest. All pristine and blended layers of NP and polymers were modelled using a multi sample analysis (MSA) procedure [14] of two coupled models of both substrate configurations. By this MSA unique fit results could be obtained for all films.

3 RESULTS

3.1 Optical constants of pristine components

The optical constants (OC) of the pristine films were modelled by Kramers-Kronig (KK) consistent generalised oscillator models. The spin-cast films were subsequently annealed, using the same conditions as for optimised solar cell performance of their respective blend films. For P3HT and PCPDTBDT and their blends this was 15 min at 140 °C, and for PCPDTBT and its blends it was 20 min at 210 °C.

The QD and NR films showed isotropic OC. The extinction coefficient (k) is illustrated in Fig.1, the index of refraction (n) is obtained by KK-relation. For the polymers uniaxial anisotropic OC were found. Within the plane parallel to the surface of the film (xy) the OC have the same values. In z-direction along the layer thickness the OC differ from the results in xy-plane. Both components are illustrated in Fig.2. Zhokhavets et al. denoted the ratio of the amplitudes of xy- and z-component as anisotropy [13]. They also reported that the higher the anisotropy the stronger is the alignment of the polymer backbones parallel to the xy-plane. The anisotropy was reported to be depending on film thickness and substrate surface energy [13]. All polymer films reported here have a layer thickness of approximately 70 nm.

3.2 EMA-modelling the blends

For blended films of polymers and NP it was reported

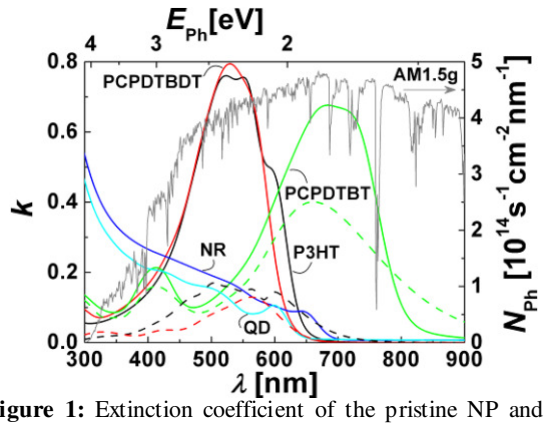

Figure 1: Extinction coefficient of the pristine NP and polymer films with layer thickness of approximately 90 nm and 70 nm, respectively. The polymers show uniaxial anisotropic behaviour with stronger extinction in the plane parallel to the surface (solid) as compared to the perpendicular direction (dashed). Isotropic OC were found for the NP-films.

that the absorption spectra equal a superposition of the pristine components [6]. This was also reported for P3HT blends with fullerene derivates [15].

Thus, the OC of blend films can be represented by effective medium theory, were the blend is described by the properties of the components weighted by volume fraction. Mass- (m) and volume ratio (v) are defined as:

$$m = \frac{m_{poly}}{m_{NP}} \quad ; \quad v = \frac{v_{poly}}{v_{NP}}, \qquad (1)$$

where m_{poly} and m_{NP}, and v_{poly} and v_{NP} are the mass and volume fractions of the polymer and NP species within the blend, respectively. The masses are determined by weighting the solvents of known concentration prior to blending.

Again the optical data of both substrate configurations were modelled in a MSA. The xy- and z-component of the OC were represented as an EMA of the polymer and NP properties in the related directions. The volume ratio was a variable fit parameter. The models showed mathematical unique results and good agreement with measured data.

3.3 Gradients of the composition

The fit quality further improved for gradients of the volume ratio along the layer thickness of the blend films. All gradients are represented by stepwise change of v. The number of steps is increased until no further improvement of model quality was obtained. Typically 3 to 8 steps were sufficient.

Linear gradients between bottom and top of the blend film are the simplest approach and where previously applied to similar problems [15]. However, van Bavel et al. showed rather complex gradients in similar films by high resolution electron tomography techniques [16,17]. For the presented samples linear, exponential and Gaussian shaped gradients were tested. All gradients showed improved fit quality as compared to the gradient-free case. Exponential and Gaussian gradients showed an even better agreement with the experimental data. However, the parameters describing the gradient showed strong correlation in both cases. Thus, no unique fit result could be obtained for the Gaussian and exponential gradient and, therefore, they were discarded. The linear gradient presented correlation free model results. For a

clear comparability the gradient is parameterized by:

$$G_{lg} = \lg\left(v_{bottom} / v_{top}\right) \quad , \qquad (2)$$

where v_{bottom} and v_{top} are the polymer volume fraction at the interface to the substrate (bottom) and the ambient (top), respectively.

Fig.2 presents the results for the G_{lg} for blends of different concentration of the polymers and the pyridine capped QD. In P3HT lower polymer concentration was found at the substrate interface, going to higher concentration at the interface to the ambient. In PCPDTBT and PCPDTBDT the gradients are in opposite direction. For all blends the gradient is strongest for the blends of lowest polymer fraction. Comparing the gradients with the optical constants of Fig.1 shows, that polymers with strong gradients also show larger degree of anisotropy.

In solar cells of such blends, the polymer is the hole-conducting species and the interface to the substrate (bottom) is the hole-contact. In case of a solar cell a metal contact is placed at the interface to the ambient (top) as a contact for electrons. Thus, it is expected that $G_{lg}>0$ exhibit better transport quality of free charges. For $G_{lg}<0$ the low polymer concentration at the hole contact acts as a barrier for holes, and the high polymer concentration at the electron contact acts as a blocking layer for electrons.

In order to verify the gradients, high resolution transmission electron microscopy (TEM) was applied. Therefore, a focused ion beam was used to prepare a thin lamella out of the area of the optical measurement spots. Fig.3 presents an overview of such a lamella. The inset shows the lattice planes of the CdSe QD, indicating a lamella thickness of only several tenths of nanometers. As confirmed by nanospot energy dispersive x-ray measurements (EDX) bright regions are rich in polymers and dark regions rich in QD species.

In order to evaluate eventual gradients a contrast limit was defined to separate polymer- and QD-rich pixels in the TEM images. This contrast limited was adjusted to fit the result of v from the respective EMA models of the samples. Finally the TEM-gradient was determined by the mean values of several high resolution images along the prepared lamella of each sample. Fig.4 shows the results of the EMA- and TEM-gradients together with representative TEM images. The profiles obtained by TEM are not linear. They rather show a strong increase of polymer concentration at one of the interfaces, similar to the results of Bavel et al. [16,17]. However, similar gradients showed better agreement of the EMA model with measured optical data, but where sorted out due to non-unique fit results. In any case, the modelled direction of the EMA-gradient agrees with the TEM results.

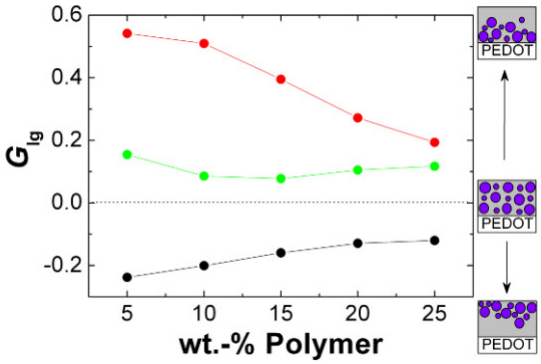

Figure 2: Logarithmic gradient of the polymer/QD volume composition for P3HT (black), PCPDTBDT (red) and PCPDTBT (green) blended with pyridine-capped QD. On the right a schematic representation of the gradient is shown (gray=QD, purple=polymer).

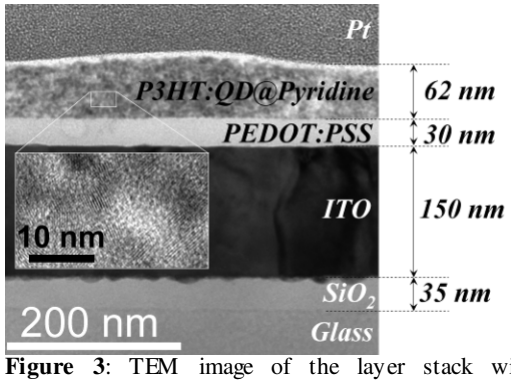

Figure 3: TEM image of the layer stack with a photoactive layer of P3HT blended with pyridine-capped QD (*m*=1:9). The blend film shows a bright, polymer rich region at the interface to the metal back contact.

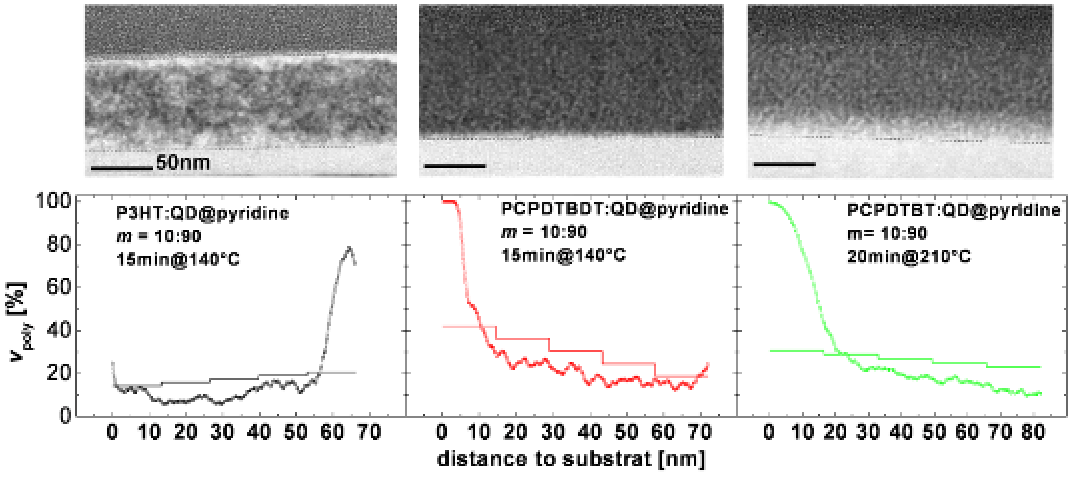

Figure 4: *bottom:* TEM- (circles) and EMA-gradient (lines) of the polymer:NP composition along the layer thickness. The TEM-gradient is a mean result of 8 (P3HT), 4 (PCPDTBDT) and 6 (PCPDTBT) images. *top:* representative TEM images of the blend films. The gradient was analysed in the area between the dotted lines.

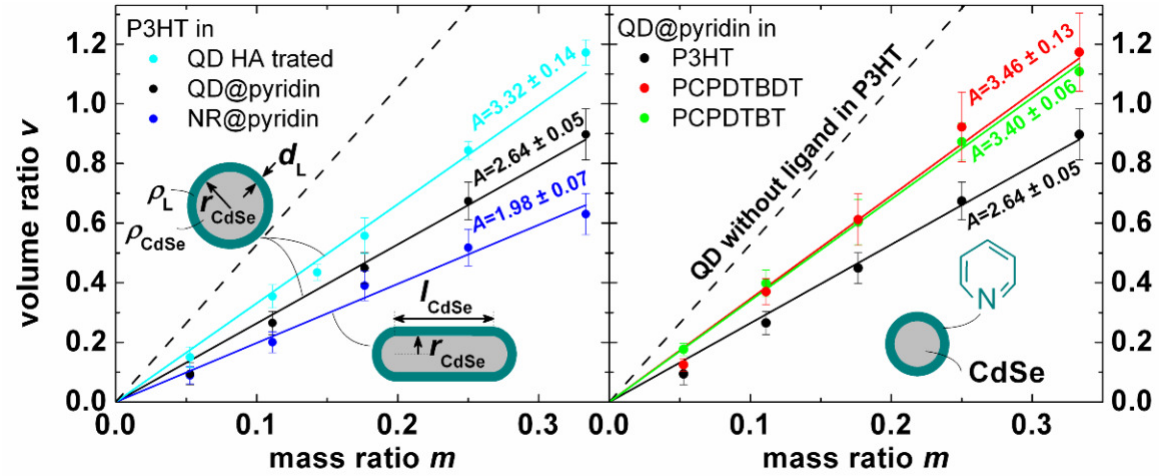

Figure 5: Volume ratio of the polymer-nanoparticle blends as derived using EMA models on optical measurements. The slope of the linear trend (*A*) equals the mass-density-ratio nanoparticles:polymer. Right: blends of pyridine capped QD with different polymers. Differences in the slope comprise information on mass densities of the polymers. The dashed line is the upper limit for the case that CdSe particles without ligand are blended with P3HT. Left: different nanoparticles blended with P3HT. Here, the different slopes comprise information on the mass densities of the particles, mainly influenced by their capping ligand layer.

3.4 Volume ratio

During the processing of organic solar cells the volume ratio is an inaccessible parameter. However, v comprises important information for the understanding of light absorption and the transport of holes and electrons within those blends. The best solar cells are reported for mass ratios between 1:9 and 3:17 [5-7, 11]. For m = 1:9 the resulting volume ratio is estimated to be v = 1:1 [18]. This volume ratio is also known from polymer:fullerene solar cells to result in good power efficiencies [15].

With the shown EMA-modelling procedure it is possible to determine the resulting mean volume ratio of the blend. Fig. 5 presents the resulting values for different NP blended with P3HT and for different polymers blended with the same NP species. As can be seen, the resulting volume ratio depends on the blended species. In all cases, for m=1:9 the resulting v is far from 1:1. The linear slope equals the ratio of mass densities ρ_{NP} / ρ_{poly}. For P3HT the dried film mass density was reported to be 1.1 gcm^{-3} [17]. Starting with this information the mass densities of the other species can be identified by the relation of the slopes of $v(m)$. For the case of a capping ligand free NP, the mass density of CdSe (5.81 gcm^{-3}) can be assumed for ρ_{NP}. In this case the maximal value for v is obtained, indicated as dashed lines in Fig. 5. For particles with an organic capping layer ρ_{NP} will further reduce and v will decrease for the same m. Even for the upper limit the volume ratio stays behind the value of 1:1 reported in literature [18].

A result of this discussion is, that for good polymer:NP solar cells a rather large amount of the film must be filled with nanoparticles. This indicates the limited ability of the NP to form efficient transport networks for the electrons to reach the electrodes. With respect to Fig.1 the absorption of sun light in the NP is by far weaker than for the polymer component. Thus, a high NP concentration in the photoactive layer causes weaker light harvesting and current densities.

3.5 Ligand layer thickness

From Fig. 5 it is obvious, that the mass density of the NP depends on the shape and the ligand species. Qualitatively, larger ligand layers and smaller CdSe crystals will cause decreasing slopes in this plot. This information can be quantified, using a geometrical model. Assuming the spherical QD to consist of a CdSe core of radius r_{CdSe} and mass density ρ_{CdSe}, and a ligand shell of layer thickness d_L and mass density ρ_L an equation for d_L can be found:

$$d_L(\rho_L) = r_{CdSe}\left(\sqrt[3]{\frac{\rho_L - \rho_{CdSe}}{\rho_L - A\rho_{poly}}} - 1\right). \qquad (3)$$

The model assumes that the blend film is a real two-component system and no unbound ligands, extant solvent or voids are left. The slope A is given by the $v(m)$-plot in Fig. 5. The radius of the CdSe crystal can be obtained by the long wavelength absorption peak [19, 20]. For the pyridine capped particles a r_{CdSe} of 2.25 nm and for the particles with the HA treated HDA ligand 2.85 nm were found. Thus in Eq.(3) only the mass density of the ligand is an unknown parameter. ρ_L will strongly depend on binding angle an packing density of the ligand species on the NP surface. Thus ρ_L is expected to differ from the values of the pristine solid or liquid ligand.

In order to indentify d_L a second independent information is required. This could be obtained by investigating the same ligand on another shape, material or size of the particle. The result for d_L and ρ_L could then be identified by the intersection of the different $d_L(\rho_L)$ plots. We used NR with the same ligand species in order to get unique results for the pyridine capping layer. In order to find a function $d_L(\rho_L)$ for the NR another geometrical model was used. It assumes the particles to be composed of a CdSe cylinder of radius r_{CdSe} and length l_{CdSe} capped with half-spheres at the ends. The ligand is built by a hollow cylinder and the sphere shells, again with layer thickness d_L and mass density ρ_L. The resulting equation for $d_L(\rho_L)$ is:

$$d_L(\rho_L) = -\frac{1}{12\sqrt[3]{2}}z - \frac{3l_{CdSe}^2}{2^{5/3}z} - r_{CdSe} - \frac{l_{CdSe}}{4}, \qquad (4)$$

with

$$z = \left[\sqrt{\left(-1296 g l_{CdSe} r_{CdSe}^2 - 1728 g r_{CdSe}^3 + 54 l_{CdSe}^3\right)^2 - 2916 l_{CdSe}^6} \right.$$
$$\left. - 1296 g l_{CdSe} r_{CdSe}^2 - 1728 g r_{CdSe}^3 + 54 l_{CdSe}^3 \right]^{1/3}$$

and

$$g = \frac{\rho_L - \rho_{CdSe}}{\rho_L - A\rho_{poly}} .$$

Again A is the slope of the $v(m)$-plot. For a NR length of 0 Eq.(4) changes to Eq.(3).

Fig.6 shows the results of $d_L(\rho_L)$ for the spherical and rod shaped particles capped with pyridine. Within the expected interval for ρ_L no point of interception can be found. In fact, the ligand seems to form much thicker layers on the NR. This might be due to a rather incomplete ligand exchange process, where a larger part of the long synthesis ligand TOP/OA is left on the NR surface. Another reason could be a smaller packing density of the NR in combination with extant ligands or solvent within the interspaces of NR-domains. Further studies are required in order to obtain unique results.

However, if the ligand layer is thin, the mass density ρ_L has a rather weak impact on the result of d_L. This can be seen by Eqs.(3) and (4): as long as $\rho_{CdSe} >> \rho_L$ and $A\rho_{poly} >> \rho_L$ the root terms show only slight dependency on ρ_L. The same can be seen in Fig.6, where $d_L(\rho_L)$ has a rather small slope within the expected range of ρ_L. Assuming the ligand to have a mass density typical for metal-free polymers of ρ_L=1±0.2 gcm^{-3} the ligand layer thickness can be obtained within an interval of approximately ±10%. With this assumption pyridine is found to form 0.8 nm on QD and 3.0 nm on NR. The HA treated HDA was found to form 0.6 nm thick layers on QD.

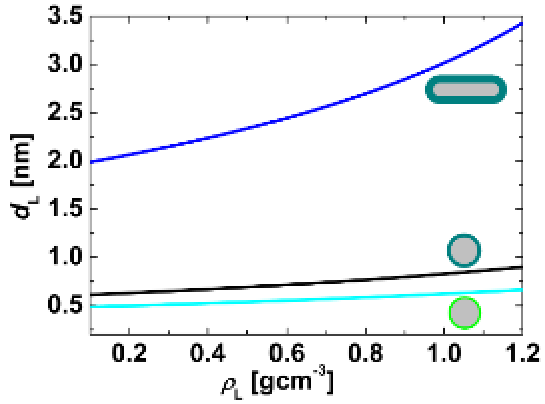

Figure 6: Ligand layer thickness as a function of its mass density. The plots result from the slope of the corresponding $v(m)$-trends and a geometrical representation of the particles in the blend with P3HT.

4 CONCLUSION

The presented methods allow for the characterisation of volume fractions and gradients of the composition along the layer thickness of polymer:nanoparticle blend films. The found volume ratio is in the range of 0.2 and 0.6 for blends optimised on solar cell efficiency. These results lie far below estimations found in literature, indicating a rather poor electron transport quality of the NP regime. The combination of volume and mass ratio comprises information on the mass density of the NP capping ligand. Using geometrical representations this leads to a measure of the ligand layer thickness.
The presented results demonstrate new information on the blend film morphology and will help for a better understanding of optical and electrical processes within such solar cells.

5 ACKNOLEDGEMENT

Financial support by the German Federal Ministry of Education and Research, reference “NanoPolySol” (03X3517B) is gratefully acknowledged. The authors want to thank the Scherf-group of University Wuppertal for providing the polymers, Dr. Phenwisa Niyamakom of Bayer Technology Services for providing the pyridine-capped particles and Dr. Lutz Berthold of the Fraunhofer IWMH for the acquisition of TEM images.

6 REFERENCES

[1] Green, M. A.; Emery, K.; Hishikawa, Y.; Warta, W. *Prog. Photovolt: Res. Appl.* **2011**, 19, 84-92
[2] Dennler, G.; Scharber, M. C.; Brabec, C. J. *Adv. Mater.* **2009**, 21, 1323-1338
[3] Alivisatos, A. P. *Science* **1996**, 271 (5251), 933-937
[4] Greenham, N. C.; Peng, X.; Alivisatos, A. P. *Phys. Rev. B* **1996**, 54 (24), 17628
[5] Zhou, Y.; Eck, M.; Veit, C.; Zimmermann, B.; Rauscher, F.; Niyamakom, P.; Yilmaz, S.; Dumsch, I.; Allard, S.; Scherf, U.; Krüger, M. *Sol. Energy Mat. Sol. Cells*, **2011**, 95, 1232-1237
[6] Dayal, S.; Kopidakis, N.; Olson, D. C.; Ginley, D. S.; Rumbles, G. *Nano Lett.*, **2010**, 10, 239-242
[7] Jeltsch, K. F.; Schädel, M.; Bonekamp, J.-B.; Meerholz, K. *E-MRS Spring Meeting*, Nice, France **2011**.
[8] Chan, E. M.; Mathies, R. A.; Alivisatos, A. P. *Nano Lett.* **2003**, 3 (2), 199-201.
[9] Liu, J.; Tanaka, T.; Sivula, K.; Alivisatos, A. P.; Frechet, J. M. J. *J. Am. Chem. Soc.* **2004**, 126, 6550-6551.
[10] Niyamakom, P. (Bayer Technology Services GmbH) EP10176561 *Patent application* (on pending)
[11] Zhou, Y.; Riehle, F. S.; Yuan, Y.; Schleiermacher, H.-F.; Niggemann, M.; Urban, G. A.; Krüger, M. *Appl. Phys. Lett.* **2010**, 94, 013304
[12] Zhu, Z.; Waller, D.; Gaudiana, R.; Morana, M.; Mühlbacher, D.; Scharber, M.; Brabec, C. J. *Macromolecules* **2007**, 40, 1981-1986
[13] Zhokhavets, U.; Gobsch, G.; Hoppe, H.; Sariciftci, N.S. *Synt. Met.* **2003**, 143, 113–117
[14] McGahan, W.A.; Johs, B.; Woollam, J.A. *Thin Solid Films* **1993**, 234, 443–446,
[15] Campoy-Quiles, M.; Ferenczi, T.; Agostinelli, T.; Etchegoin, P. G.; Kim, Y.; Anthopoulos, T. D.; Stavrinou, P. N.; Bradley, D. D. C.; Nelson, J. *Nat. Mater.* **2008**, 7, 158-164
[16] van Bavel, S.; Loos., J. *Adv. Funct. Mater.*, 20(19):3217–3234, 2010.
[17] van Bavel, S.; Bärenklau, M.; De With, G.; Hoppe, H.; Loos. J. *Adv. Funct. Mater.*, 20(9):1458–1463, 2010.
[18] Greenham, N. C. Organic Photovoltaics; Brabec, C.; Dyankonov, V.; Scherf, U. Eds.; WILEY-VCH Verlag GmbH & Co KGaA, Weinheim, Germany **2008**, Ch. 6
[19] Yu, W. W.; Qu, L.; Guo, W.; Peng, X. *Chem. Mater.* **2003**, 15, 2854–2860
[20] Jasieniak, J.; Smith, L.; van Embden, J.; Mulvaney, P. *J. Phys. Chem.* **2009**, 113, 19468–19474